Journal of Solid State Chemistry 183 (2010) 471–478

Contents lists available at ScienceDirect

Journal of Solid State Chemistry

journal homepage: www.elsevier.com/locate/jssc

$Gd_4B_4O_{11}F_2$: Synthesis and crystal structure of a rare-earth fluoride borate exhibiting a new "fundamental building block" in borate chemistry

Almut Haberer [a], Reinhard Kaindl [b], Hubert Huppertz [a,*]

[a] Institut für Allgemeine, Anorganische und Theoretische Chemie, Leopold-Franzens-Universität Innsbruck, Innrain 52a, A-6020 Innsbruck, Austria
[b] Institut für Mineralogie und Petrographie, Leopold-Franzens-Universität Innsbruck, Innrain 52, A-6020 Innsbruck, Austria

ARTICLE INFO

Article history:
Received 3 July 2009
Received in revised form
24 November 2009
Accepted 7 December 2009
Dedicated to Dr. Klaus Römer on the Occasion of His 70th Birthday
Available online 16 December 2009

Keywords:
High-pressure
Multianvil
Crystal structure
Fluoride borate

ABSTRACT

A new gadolinium fluoride borate $Gd_4B_4O_{11}F_2$ was yielded in a Walker-type multianvil apparatus at 7.5 GPa and 1100 °C. $Gd_4B_4O_{11}F_2$ crystallizes monoclinically in the space group $C2/c$ with the lattice parameters a=1361.3(3) pm, b=464.2(2) pm, c=1374.1(3) pm, and β=91.32(3)° (Z=4). The crystal structure exhibits a structural motif not yet reported from borate chemistry: two BO_4-tetrahedra (□) and two BO_3-groups (△) are connected via common corners, leading to the fundamental building block 2△2□:△□□△. In the two crystallographically identical BO_4-tetrahedra, a distortion resulting in a very long B–O-bond is found.

1. Introduction

The possibility to obtain a large variety of new compounds under high-pressure/high-temperature conditions has been extensively studied for borates, for example the rare-earth borates $RE_4B_6O_{15}$ (RE=Dy, Ho) [1–3], α-$RE_2B_4O_9$ (RE=Sm–Ho) [4–6], β-$RE_2B_4O_9$ (RE=Gd [7], Dy [8]), $RE_3B_5O_{12}$ (RE=Er–Lu) [9], $Pr_4B_{10}O_{21}$ [10], and the *meta*-borates β-$RE(BO_2)_3$ (RE=Tb–Lu) [11–13], γ-$RE(BO_2)_3$ (RE=La–Nd) [14], and δ-$RE(BO_2)_3$ (RE=La, Ce) [15,16].

Until recently, the field of rare-earth fluoride borates was only represented by the compounds $RE_3(BO_3)_2F_3$ (RE=Sm, Eu, Gd) [17] and $Gd_2(BO_3)F_3$ [18], which were synthesized by heating a stoichiometric mixture of RE_2O_3, B_2O_3, and REF_3 under ambient pressure conditions. Under high-pressure/high-temperature conditions, the first ytterbium fluoride borate $Yb_5(BO_3)_2F_9$ could be added to the field by our group [19].

Borates, being glass formers in general, show an increased willingness to crystallize under pressure, which seems to hold true for fluoroborates, too. The chemistry of rare-earth fluoride borates under high-pressure/high-temperature conditions shows similarities to the chemistry of the borates concerning structural motifs. Trigonal-planar BO_3-groups as well as BO_4-tetrahedra can be identified and the pressure-induced transformation of the former into the latter can be observed. The application of higher pressures on $Yb_5(BO_3)_2F_9$, which exhibits only BO_3-groups, yielded a structure built up solely from BO_4-tetrahedra [20]. The motif of edge-sharing tetrahedra could be realized under high pressure for the compounds $RE_4B_6O_{15}$ (RE=Dy, Ho) [1–3] and α-$RE_2B_4O_9$ (RE=Sm–Ho) [4–6]. Recently, HP–NiB_2O_4 [21] and β-FeB_2O_4 [22] were synthesized, in which each BO_4-tetrahedron shares a common edge with another tetrahedron. For fluoro- and fluoride borates, this structural feature is not known yet.

In this article, we present a new gadolinium fluoride borate $Gd_4B_4O_{11}F_2$, obtained by high-pressure/high-temperature synthesis. In the crystal structure of $Gd_4B_4O_{11}F_2$, BO_3-groups as well as BO_4-tetrahedra are found, connected via common corners. In borate chemistry, the polyhedral B–O-clusters are described according to their linkage. Hawthorne et al. distinguish several fundamental building blocks (FBBs), that are known to be found in borates, consisting of specific arrangements of BO_3-groups and BO_4-tetrahedra [23]. In $Gd_4B_4O_{11}F_2$, the polyhedra form a FBB not yet reported from borate chemistry. The structural motif consists of two BO_3-groups (△) and two BO_4-tetrahedra (□) and can be described with the fundamental building block 2△2□:△□□△ (after Burns et al. [24]). The two crystallographically identical tetrahedra in the FBB are distorted, showing a very long B–O-bond. A closer look reveals that the coordination sphere of the boron atom can be described as an intermediate state between a BO_3-group and a BO_4-tetrahedron. In the following, synthesis and structural details of the new compound $Gd_4B_4O_{11}F_2$ are reported.

* Corresponding author. Fax: +435125072934.
E-mail address: hubert.huppertz@uibk.ac.at (H. Huppertz).

0022-4596/$ - see front matter © 2009 Elsevier Inc. All rights reserved.
doi:10.1016/j.jssc.2009.12.003

2. Experimental section

2.1. Synthesis

The synthesis of the fluoride borate $Gd_4B_4O_{11}F_2$ took place under high-pressure/high-temperature conditions of 7.5 GPa and 1100 °C. Therefore, a mixture of Gd_2O_3 (Strem Chemicals, 99.99%), B_2O_3 (Strem Chemicals, 99.9+%), and GdF_3 (Strem Chemicals, 99.9%) at a molar ratio of 5:6:2 was ground and filled into a boron nitride crucible (Henze BNP GmbH, HeBoSint® S10, Kempten, Germany). This crucible was placed into the center of an 14/8-assembly, which was compressed by eight tungsten carbide cubes (TSM-10 Ceratizit, Reutte, Austria). The details of preparing the assembly can be found in Refs. [25–29]. Pressure was applied by a multianvil device based on a Walker-type module and a 1000 ton press (both devices from the company Voggenreiter, Mainleus, Germany). The sample was compressed up to 7.5 GPa in 3 h, then heated to 1100 °C in 15 min and kept there for 20 min. Afterwards, the sample was cooled down to 850 °C in 20 min, followed by natural cooling down to room temperature by switching off heating. The decompression required 9 h. The recovered experimental MgO-octahedron (pressure transmitting medium, Ceramic Substrates & Components Ltd., Newport, Isle of Wight, UK) was broken apart and the sample carefully separated from the surrounding boron nitride crucible, obtaining colorless, air- and water-resistant, crystal platelets of $Gd_4B_4O_{11}F_2$.

2.2. Crystal structure analysis

Sample characterization was performed by powder X-ray diffraction, carried out in transmission geometry on a flat sample of the reaction product, using a STOE STADI P powder diffractometer with Mo$K\alpha_1$ radiation (Ge monochromator, λ=71.073 pm). The powder pattern showed reflections of $Gd_4B_4O_{11}F_2$, as well as of α-$Gd_2B_4O_9$ [5] as a by-product of the synthesis. The experimental powder pattern tallies well with the theoretical patterns of the two compounds, simulated from single-crystal data. Indexing the reflections of the gadolinium fluoride borate, we got the parameters a=1362.4(4) pm, b=464.2(3) pm, and c=1374.8(5) pm, with β=91.18(3)° and a volume of 869.2(4) Å^3. This confirmed the lattice parameters, obtained from single-crystal X-ray diffraction (Table 1).

The intensity data of a single crystal of $Gd_4B_4O_{11}F_2$ were collected at room temperature by the use of a Kappa CCD diffractometer (Bruker AXS/Nonius, Karlsruhe), equipped with a Miracol Fiber Optics Collimator and a Nonius FR590 generator (graphite-monochromatized Mo$K\alpha_1$ radiation, λ=71.073 pm). A multi-scan absorption correction (Scalepack [30]) was applied to the intensity data. All relevant details of the data collection and evaluation are listed in Table 1.

Structure solution and parameter refinement (full-matrix least-squares against F^2) were successfully performed, using the SHELX-97 software suite [31,32] with anisotropic atomic displacement parameters for all atoms. According to the systematic

Table 1
Crystal data and structure refinement of $Gd_4B_4O_{11}F_2$.

Empirical formula	$Gd_4B_4O_{11}F_2$
Molar mass (g mol^{-1})	812.87
Crystal system	Monoclinic
Space group	$C2/c$ (no.15)
Lattice parameters from powder data	
Powder diffractometer	Stoe Stadi P
Radiation	Mo$K\alpha_1$ (λ=71.073 pm)
a (pm)	1362.4(4)
b (pm)	464.2(3)
c (pm)	1374.8(5)
β (deg)	91.18(3)
Volume (Å^3)	869.2(4)
Single-crystal diffractometer	Bruker AXS/Nonius Kappa CCD
Radiation	Mo$K\alpha_1$ (λ=71.073 pm)
Single-crystal data	
a (pm)	1361.3(3)
b (pm)	464.2(2)
c (pm)	1374.1(3)
β (deg)	91.32(3)
Volume (Å^3)	868.1(3)
Formula units per cell	Z=4
Temperature (K)	293(2)
Calculated density (g cm^{-3})	6.781
Crystal size (mm^3)	0.03 × 0.02 × 0.02
Absorption coefficient (mm^{-1})	30.266
F (000)	1528
θ range (deg)	$2.97 \le \theta \le 30.00$
Range in $h\,k\,l$	±18, ±6, ±19
Total no. reflections	4570
Independent reflections	1271 (R_{int}=0.0310)
Reflections with $I > 2\sigma$(I)	1094 (R_σ=0.0262)
Data/parameters	1271/97
Absorption correction	Multi-scan
Goodness-of-fit (F^2)	1.114
Final R indices ($I > 2\sigma(I)$)	$R1$=0.0205
	w$R2$=0.0359
R indices (all data)	$R1$=0.0287
	w$R2$=0.0377
Largest differ. peak / deepest hole (e/Å^{-3})	0.93/−0.90

Table 2
Atomic coordinates and isotropic equivalent displacement parameters (U_{eq}/Å^2) for $Gd_4B_4O_{11}F_2$ (space group: $C2/c$).

Atom	Wyckoff site	x	y	z	U_{eq}
Gd1	8f	0.05835(2)	0.52008(5)	0.37047(2)	0.00601(7)
Gd2	8f	0.27992(2)	0.01782(5)	0.37101(2)	0.00577(7)
B1	8f	0.9072(4)	0.978(2)	0.2849(4)	0.0054(9)
B2	8f	0.0954(4)	0.957(2)	0.5235(4)	0.008(1)
O1	8f	0.9129(2)	0.8649(6)	0.3942(2)	0.0055(6)
O2	8f	0.1745(2)	0.8173(7)	0.2568(2)	0.0068(7)
O3	8f	0.0792(2)	0.6640(7)	0.5339(2)	0.0063(7)
O4	4e	0	0.8460(9)	$\frac{1}{4}$	0.0047(9)
O5	8f	0.1145(3)	0.0621(7)	0.4334(3)	0.0089(7)
O6	8f	0.9015(3)	0.2807(7)	0.2765(2)	0.0070(7)
F1	8f	0.2312(2)	0.5248(6)	0.4236(2)	0.0149(6)

U_{eq} is defined as one-third of the trace of the orthogonalized U_{ij} tensor.

Table 3
Interatomic distances (pm) in $Gd_4B_4O_{11}F_2$, calculated with the single-crystal lattice parameters.

Gd1–O3a	235.4(3)	Gd2–O2a	230.0(3)	B1–O6	141.3(6)	B2–O5	136.1(6)
Gd1–O4	236.6(3)	Gd2–O2b	233.4(3)	B1–O2	144.7(6)	B2–O3	138.8(6)
Gd1–O6a	237.9(3)	Gd2–O6	239.5(3)	B1–O4	149.3(5)	B2–O1	140.7(6)
Gd1–O5a	241.3(3)	Gd2–O5	243.6(3)	B1–O1	159.0(6)		
Gd1–F1	244.8(3)	Gd2–O1	243.9(3)		∅ **=148.6**		∅ **=138.5**
Gd1–O3b	246.5(3)	Gd2–O3	244.6(3)				
Gd1–O1	257.2(3)	Gd2–F1a	249.5(3)	F1–Gd1	244.8(3)		
Gd1–O2	263.8(3)	Gd2–F1b	255.4(3)	F1–Gd2a	249.5(3)		
Gd1–O6b	270.8(4)	Gd2–F1c	283.7(3)	F1–Gd2b	255.4(3)		
Gd1–O5b	276.3(3)			F1–Gd2c	283.7(3)		
	∅ **=251.0**		∅ **=247.1**		∅ **=258.4**		

Table 4
Interatomic angles (deg) in $Gd_4B_4O_{11}F_2$, calculated with the single-crystal lattice parameters.

O1–B1–O2	102.9(3)	O1–B2–O3	118.5(4)	Gd1–F1–Gd2a	99.3(2)
O1–B1–O4	98.3(3)	O1–B2–O5	122.8(4)	Gd1–F1–Gd2b	100.5(2)
O1–B1–O6	114.1(4)	O3–B2–O5	118.6(4)	Gd1–F1–Gd2c	102.9(2)
O2–B1–O4	108.0(4)		∅ = **120.0**	Gd2a–F1–Gd2b	133.7(2)
O2–B1–O6	116.1(4)			Gd2a–F1–Gd2c	103.7(2)
O4–B1–O6	115.3(4)			Gd2b–F1–Gd2c	111.9(2)
	∅ = **109.1**				∅ = **108.7**

extinctions, the monoclinic space groups $C2/c$ and Cc were derived. The structure solution in $C2/c$ (no. 15) succeeded. The final difference Fourier syntheses did not reveal any significant residual peaks in all refinements. The positional parameters of the refinements, interatomic distances, and interatomic angles are listed in Tables 2–4. Further information of the crystal structure is available from the Fachinformationszentrum Karlsruhe (crysdata@fiz-karlsruhe.de), D-76344 Eggenstein-Leopoldshafen (Germany), quoting the registry no. CSD-420809.

2.3. Scanning electron microscopy

Scanning electron microscopy was performed on a JEOL JSM-6500F equipped with a field emission gun at an acceleration voltage of 15 kV. Samples were prepared by placing single crystals on adhesive conductive pads and subsequently coating them with a thin conductive carbon film. Each EDX spectrum (Oxford Instruments) was recorded with the analyzed area limited on one single crystal to avoid the influence of possible contaminating phases.

2.4. IR spectroscopy

FTIR absorption transmission spectra of the crystals were recorded on a BaF_2 plate with a Bruker Vertex 70 FT-IR spectrometer (resolution $\sim 0.5\,cm^{-1}$) attached to a Hyperion 3000 microscope in a spectral range from 550 to $4000\,cm^{-1}$. A quadrangular diaphragm was set to a diameter of 100 μm for both spectrum and background measurement. For background correction, polynomial functions of second order were fitted to the spectra and subtracted. A rotatable polarizer was used to define a certain orientation of the electric field vector of the incoming IR light.

2.5. Raman spectroscopy

Confocal Raman spectra of single crystals were obtained with a HORIBA JOBIN YVON LabRam-HR 800 Raman micro-spectrometer. The sample was excited using the 633 nm emission line of a 17 mW He–Ne-laser and an OLYMPUS 100 × objective (N.A. = 0.9). Size and power of the laser spot on the surface were approximately 1 μm and 5 mW. The spectral resolution, determined by measuring the Rayleigh line, was about $1.2\,cm^{-1}$. The dispersed light was collected by a 1024 × 256 open electrode CCD detector. Spectra were recorded without polarizer for the laser and the scattered Raman light. Raman bands were fitted by the built-in spectrometer software LabSpec to convoluted Gauss–Lorentz functions. Accuracy of Raman line shifts, calibrated by regular measuring the Rayleigh line, was in the order of $0.5\,cm^{-1}$.

3. Results and discussion

X-ray diffraction is a powerful tool for crystal structure solution and refinement. Nevertheless, in the chemistry of fluoride borates or fluoride minerals, it is nearly impossible to distinguish between fluoride ions and hydroxyl groups by means of electron density or bond lengths. Via crystal structure refinement, the composition $Gd_4B_4O_{11}F_2$ was determined. To assure the atom assignment in the structure, single crystals of our sample were subjected to elemental analysis. The crystals showed average atomic Gd:B:O:F compositions (%) of 14.7:20.5:53.2:11.6. Due to the light weight of boron, measurements have to be taken with caution, but still, these results confirm the presence of all elements and the composition obtained from the single crystal structure determination (calculated values (%) Gd:B:O:F: 19.0:19.0:52.5:9.5).

Due to the fact that a differentiation between fluoride anions and hydroxyl groups at a crystallographic site via structural refinement is impossible, IR-spectrocopic investigations were performed on single-crystals of the sample (Fig. 1). Looking closely at the region of 3100–$3600\,cm^{-1}$, two small peaks could be detected that hardly overtopped the background noise. Absorption bands at those wavelengths can be assigned to OH-groups and typically reveal OH-containing borates [33]. A direction-dependent measurement clearly showed that the bands are not evoked by surface humidity of the crystals but indeed by internal OH-groups. On the basis of these IR measurements, the presence of traces of OH-groups in $Gd_4B_4O_{11}F_2$ has to be assumed. The problem of hydroxyl quantification is commonly known from halogen containing minerals and often the exact composition is merely estimated, as done for $Mn_5(PO_4)_3Cl_{0.9}(OH)_{0.1}$ [34]. The title compound could therefore also be described as "$Gd_4B_4O_{11}F_{2-x}(OH)_x$". Because of the diminutive size of the OH-bands (a fraction of what is known from water- or OH-containing borates) and the results of elemental analysis, the value of x has to be considered as minimal and is therefore neglected in the structural description.

Furthermore, we calculated the Madelung Part of Lattice Energy (MAPLE) [35–37] for $Gd_4B_4O_{11}F_2$ in order to compare it with the sum of the MAPLE values of the high-temperature modifications of Gd_2O_3 [38] and GdF_3 [39], and of the high-pressure modification of B_2O_3 (B_2O_3–II) [40]. The additive

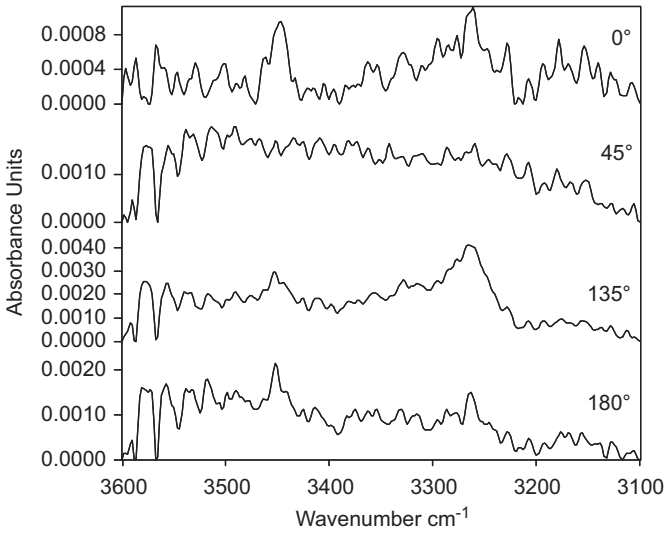

Fig. 1. Polarized IR absorption spectra of $Gd_4B_4O_{11}F_2$ in the region 3100–$3600\,cm^{-1}$. The spectra were recorded at four different angles of the electric field vector of the IR-light relative to the crystal. The weak absorption bands around 3250 and $3450\,cm^{-1}$ can be assigned to OH-groups.

potential of the MAPLE values allows the calculation of a hypothetical value for $Gd_4B_4O_{11}F_2$, starting from binary oxides and fluorides. As a result, we obtained a value of 72407 kJ/mol in comparison to 72481 kJ/mol (deviation: 0.1%), starting from the binary components [5/3 × Gd_2O_3 (14950 kJ/mol)+2 × B_2O_3–II (21938 kJ/mol)+2/3 × GdF3 (5532 kJ/mol)], which also indicates that the small amount of hydrogen groups can be neglected.

3.1. Crystal structure of $Gd_4B_4O_{11}F_2$

The structure of $Gd_4B_4O_{11}F_2$ consists of BO_3-groups, BO_4-tetrahedra, gadolinium cations, and fluoride anions (Fig. 2). The two BO_3-groups (△) and two BO_4-tetrahedra (□) are connected via common corners, forming a fundamental building block (FBB) 2△2□:Δ□□Δ, which has not yet been reported by Burns et al. [24]. In 2002, Becker summarized the FBBs known from borate structures, mentioning four compounds with the motif 2△2□:Δ□□Δ [41], namely the borates $BaBe_2(BO_3)_2$ [42], $SrCu_2(BO_3)_2$ [43], $Sr_{0.74}Ba_{0.26}Cu_2(BO_3)_2$, and $Sr_{0.66}Ca_{0.33}Cu_2(BO_3)_2$ [44]. However, in $BaBe_2(BO_3)_2$, the tetrahedra are not BO_4-tetrahedra, but BeO_4-tetrahedra, connected via common edges. For the structural motif of edge-sharing tetrahedra, our group established the new descriptor "⧄" in 2003, which extended the FBB concept [2]. Strictly speaking, the FBB descriptors according to Burns et al. are only applied to mere B–O-polyhedra. Nevertheless, if the FBB concept is applied to $BaBe_2(BO_3)_2$ after all, the correct FBB notation now should be 2△2□:△⧄△. Fig. 3 left shows the structure of $BaBe_2(BO_3)_2$ with interconnected building blocks, leading to a network structure.

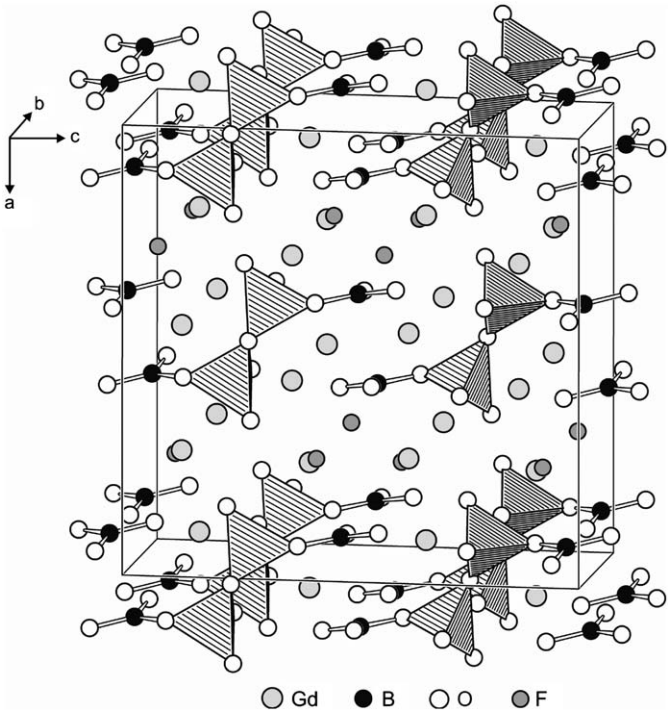

Fig. 2. Crystal structure of $Gd_4B_4O_{11}F_2$, showing the fundamental building block units consisting of BO_3-groups and BO_4-tetrahedra.

In the compounds $SrCu_2(BO_3)_2$, $Sr_{0.74}Ba_{0.26}Cu_2(BO_3)_2$, and $Sr_{0.66}Ca_{0.33}Cu_2(BO_3)_2$, there are not even tetrahedra in the structural motif; the fourfold-coordinated copper ions show square-planar geometry. This is exemplified for $Sr_{0.74}Ba_{0.26}Cu_2(BO_3)_2$ in Fig. 3 (right). The so called FBBs build up two-dimensional sheets, connected via Sr, Ba, or Ca ions.

In $Gd_4B_4O_{11}F_2$, the isolated FBBs exclusively consist of B–O-polyhedra (Fig. 2). Their locations in the unit cell are displayed in Fig. 4 (view along [00$\bar{1}$]). To the best of our knowledge, this fluoride borate is the first compound exhibiting a real 2△2□:△□□△ motif according to Burns et al. [24] and is thus extending the borate fundamental building block concept by a new structural motif.

A closer look at the new FBB of $Gd_4B_4O_{11}F_2$ is given in Fig. 5. A twofold rotation axis is running through the tetrahedra-bridging oxygen O4, thus all threefold- and fourfold-coordinated boron atoms are crystallographically identical (Table 2). Inside the BO_3-groups, the B2–O-distances range from 136.1(6) to 140.7(6) pm (Table 3), which is typical for threefold-coordinated boron atoms, e.g. in borates with calcite structure ($AlBO_3$ (137.96(4) pm) [45], β-$YbBO_3$ (137.8(4) pm) [46], and $FeBO_3$ (137.9(2) pm) [47]). The B2–O-angles sum up to 120° (Table 4), as would be expected from the trigonal-planar geometry.

Inside the BO_4-tetrahedra, the B1–O average bond lengths is 148.6 pm (Table 3) and thus fairly larger than the known average value of 147.6 pm for fourfold-coordinated boron atoms in borates [23]. The reason for this deviation can be seen in Fig. 6. The central boron atom B1 is dislocated from the center of the trigonal plane spanned up by O2, O6, and O4. In detail, the boron atom is shifted towards the oxygen atom O1 from the neighboring BO_3-group, indicating an intermediate state between a strongly distorted

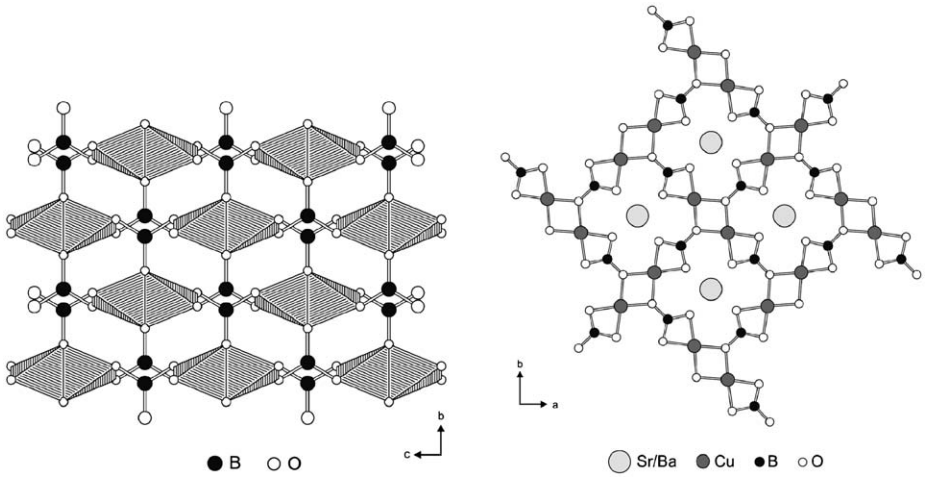

Fig. 3. Left: Structure of $BaBe_2(BO_3)_2$, showing edge-sharing BeO_4-tetrahedra, connected via BO_3-groups, resulting in a network structure. Right: Structure of $Sr_{0.74}Ba_{0.26}Cu_2(BO_3)_2$, built up from edge-sharing, square-planar CuO_4-units connected via BO_3-groups, resulting in a layered structure.

trigonal BO_3-group and a BO_4-tetrahedron. Thus, the tetrahedron could be seen as a former BO_3-group, in which the boron atom is drawn towards a fourth oxygen atom, resulting in the long B1–O1-bond of 159.0(6) pm displayed in Fig. 6. The non-planarity of BO_3-groups, due to the close proximity of another oxygen atom, is described in the literature [48]. Calculation of the coordination number of B1 with MAPLE (Madelung Part of Lattice Energy) [49–51] results in a value of 3.73, verifying the assumption of a transition state. The O–B–O angles in the BO_4-tetrahedra vary between 98.3(3)° and 116.1(4)° with a mean value of 109.1°, indicating a slight distortion.

Another point of interest in $Gd_4B_4O_{11}F_2$ are the BO_3-groups of two neighboring building blocks, facing each other at a relatively short B–B-distance of 269 pm (Figs. 7a and c). The distances of the boron atoms to the next oxygen atom outside the coordination sphere account for 292.9 pm. Similar arrangements of BO_3-groups were also found in $M_3(BO_3)_2$ (M=Mg, Co, Ni), where the B–O-distances of one boron atom to the first oxygen atom of the second BO_3-group are <260 pm [52]. In these compounds, a transition state between threefold and fourfold boron coordination is found, leading formally to two distorted BO_4-tetrahedra connected via common edges (Fig. 7b). While the B–B-distance in undistorted edge-sharing tetrahedra usually lies around 215 pm [1–6,21,22], the B–B-distance in $Mg_3(BO_3)_2$ measures 268 pm. A similar transition could be expected for $Gd_4B_4O_{11}F_2$, as exemplified in Figs. 7a and c. The application of higher pressures might transform the neighboring BO_3-groups into edge-sharing BO_4-tetrahedra, which are an extremely rare structural feature of high-pressure borates.

There are two crystallographically independent Gd^{3+} ions in the structure, which are nine-and tenfold coordinated by oxygen and fluorine (Fig. 8). Gd1 has got nine oxide ions and one fluoride ion in the coordination sphere, whereas Gd2 is surrounded by six oxide and three fluoride ions. As presented in Table 3, the average interatomic distance Gd2–O/F with 247.1 pm is in the same range as the average Gd–O/F distance of ninefold coordinated Gd^{3+} in $Gd_2[BO_3]F_3$ (242.7 pm [18]). The average distance Gd1–O/F of 251.1 pm is larger, as would be expected from a tenfold coordination.

The fluoride ion in $Gd_4B_4O_{11}F_2$ is coordinated by four gadolinium ions (Fig. 8). The bond lengths (Table 3) range between 244.8(3) and 283.7(3) pm, being in the same region as the bond lengths of the fourfold-coordinated fluoride ion in the high-temperature phase of GdF_3 (249.8–276.5 pm) [53]. The Gd–F angles sum up to 108.7° (Table 4), which is fairly close to the ideal tetrahedron angle.

The calculations of the charge distribution of the atoms in $Gd_4B_4O_{11}F_2$ via bond valence sums (ΣV) with VaList (bond valence calculation and listing) [54] and with the CHARDI (charge distribution in solids) concept (ΣQ) [55–57] confirm the formal valence states in the fluoride borate (Table 5).

The Raman spectrum of $Gd_4B_4O_{11}F_2$ is displayed in Fig. 9. A relatively large number of 38 bands from 113 to 1358 cm^{-1} could be detected (Table 6), consistent with the low symmetry of the structure. No Raman-active OH-stretching modes between 3100 and 3600 cm^{-1} (see above) were observed, which is probably caused by the low OH-content and high background in this spectral region.

Bands in the range between 800 and 1600 cm^{-1} are generally assigned to stretching vibrations of BO_4 tetrahedra and BO_3 groups [5,33,58–61]. The former ones are expected at wave numbers below, the latter ones above 1100 cm^{-1}. This is consistent with the strong band at 959 cm^{-1} and the two bands at 1244 and 1282 cm^{-1}. The large average bond length within the tetrahedra (147.6 pm, see above) results in the comparable low wave number of the vibrational mode. E.g. in $Co_6B_{22}O_{39}\cdot H_2O$ [62], which contains BO_4-tetrahedra with a mean B–O distance of 145.7 pm, the respective mode is observed at 1035 cm^{-1}. The variable B2–O-distances inside the BO_3-groups or their connection to BO_4-tetrahedra in fundamental building blocks might account for two instead of one stretching modes in this range as it was described for compounds containing isolated planar molecules (e.g. [58]).

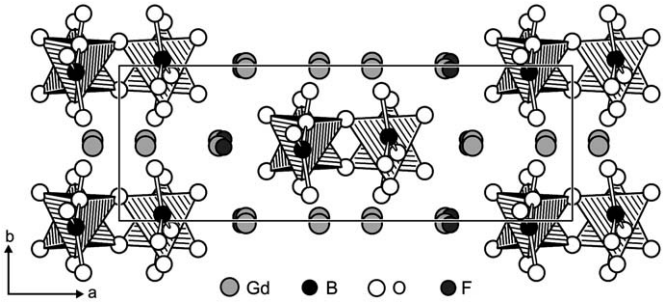

Fig. 4. Crystal structure of $Gd_4B_4O_{11}F_2$, viewing along [00$\bar{1}$].

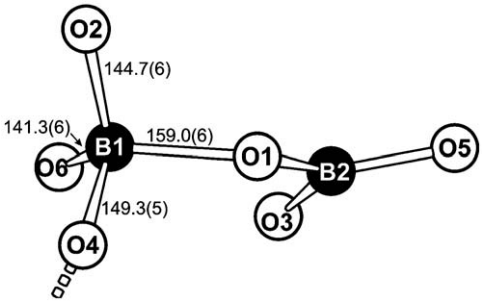

Fig. 6. Transition of B1 from a trigonal to a tetrahedral coordination, resulting in an elongated B1–O1-bond length (bond lengths in pm).

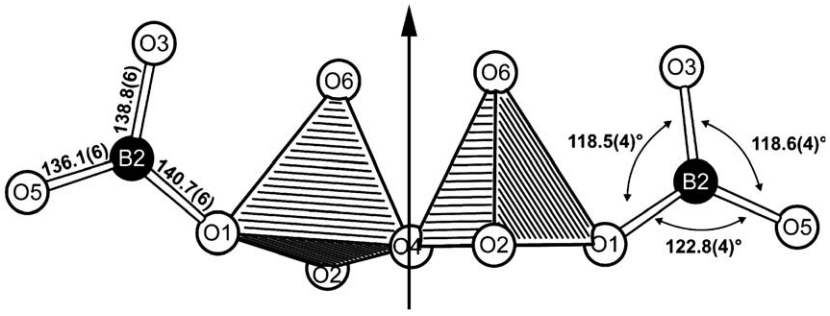

Fig. 5. Fundamental building block 2△2□:△□□△ in $Gd_4B_4O_{11}F_2$, showing a twofold rotation axis at O4 (bond lengths in pm).

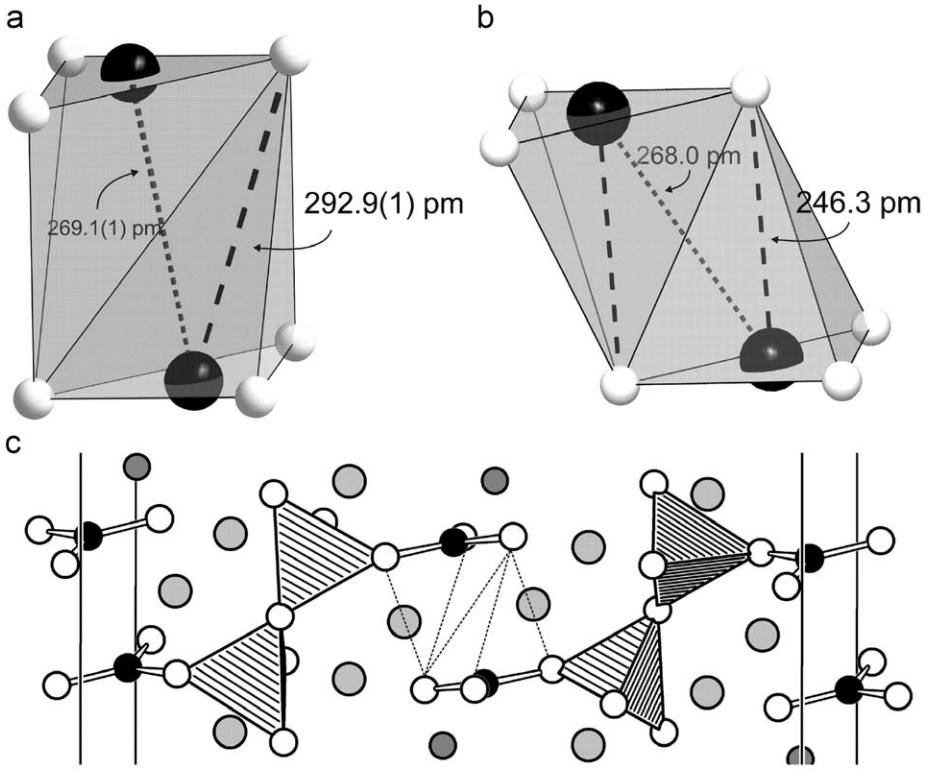

Fig. 7. (a) Possible transition of BO_3-groups into edge-sharing BO_4-tetrahedra in $Gd_4B_4O_{11}F_2$. (b) BO_3-groups in $Mg_3(BO_3)_2$ in an arrangement which could form edge-sharing BO_4-tetrahedra under elevated pressure conditions. (c) Neighboring BO_3-groups in $Gd_4B_4O_{11}F_2$ building blocks with implied edge-sharing BO_4-tetrahedra.

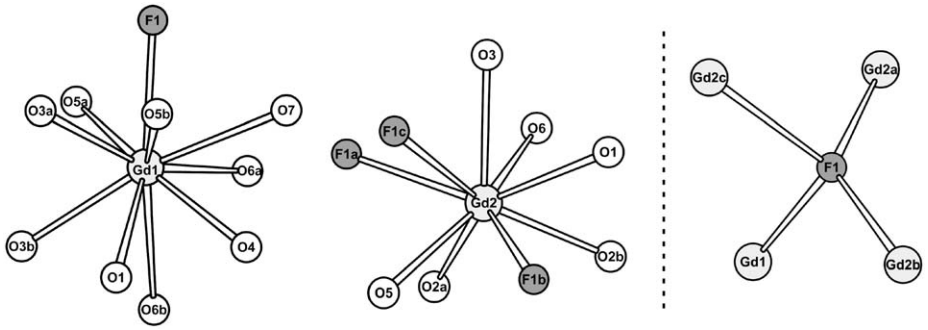

Fig. 8. Coordination spheres of the Gd^{3+} and F^- ions in $Gd_4B_4O_{11}F_2$.

Table 5
Charge distribution in $Gd_4B_4O_{11}F_2$, calculated with VaList (ΣV) and CHARDI (ΣQ).

	Gd1	Gd2	B1	B2			
ΣV	3.11	3.03	2.98	2.89			
ΣQ	2.97	3.04	2.97	3.02			
	O1	O2	O3	O4	O5	O6	F1
ΣV	−2.08	−2.04	−2.11	−2.32	−1.94	−1.91	−0.78
ΣQ	−1.92	−2.00	−2.10	−2.26	−1.95	−1.93	−0.97

After a wide spectral gap, numerous bands occur from 700 to 200 cm^{-1}, the most intense bands are observed at very low wave numbers below 200 cm^{-1}. These bands can be assigned to bending and stretching vibrations of various borate arrangements, Gd–O, F–O, and Gd–F bonds and complex lattice vibrations. In hydrated tetraborates [58], which contain a polyborate anion with two planar BO_3 triangles, two BO_4-tetrahedra, and OH-groups, very strong stretching vibrations of this unit between 543 and

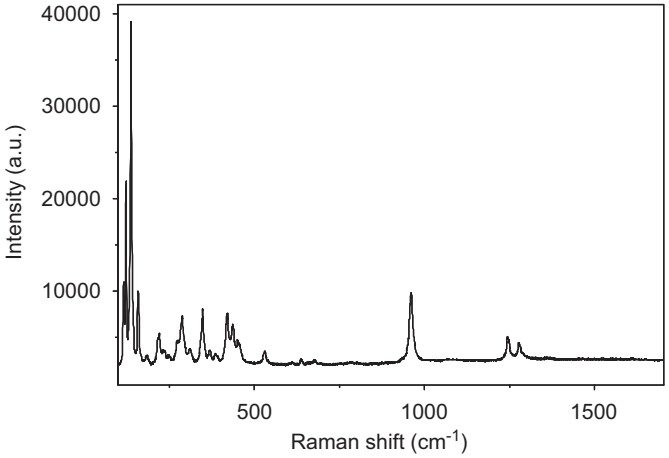

Fig. 9. Unpolarized micro-Raman spectrum of a single crystal of $Gd_4B_4O_{11}F_2$.

Table 6
Raman shifts of observed bands and tentative assignment of the spectrum of $Gd_4B_4O_{11}F_2$.

Raman shift (cm^{-1})	Assignment
113	
120	
134	
155	
158	
181	
212	
218	lattice, Gd–O, Gd–F, F–O
230	
245	
270	
285	
308	
345	
366	
383	
390	Bending (BO_4)
417	
434	
448	
455	
528	
609	
636	Pulse vibration (BO_3)–(BO_4)
660	
676	
693	
748	
785	
886	
932	Stretching (BO_4)
959	
1001	
1075	
1244	
1277	Stretching (BO_3)
1282	
1358	

583 cm^{-1} were observed, whereas bending vibrations of the tetrahedra are described around 391–461 cm^{-1}. The low wave number region was not studied by Jun et al. [58]; we believe that the very strong bands of $Gd_4B_4O_{11}F_2$ below 200 cm^{-1} are dominantly related to the fourfold-coordinated fluoride and the Gd^{3+} ion. More reliable assignments of observed bands to vibrational modes would require quantum mechanical calculations of the structure, which are not available up to now.

4. Conclusions

In this article, we described the high-pressure synthesis and crystal structure of the new gadolinium fluoride borate $Gd_4B_4O_{11}F_2$. The structure is built up from a fundamental building block 2△2□:△□□△, which has not yet been reported in borate chemistry. The tetrahedra in the structural motif are distorted, indicating a transition state between a distorted trigonal BO_3-group and a BO_4-tetrahedron. The possible transformation of neighboring BO_3-groups into edge-sharing tedrahedra is another point of interest and will be object of our further studies.

Acknowledgments

We thank Dr. Gunter Heymann for collecting the single-crystal data and Christian Minke (LMU München) for the scanning electron microscopy measurements. Special thanks go to Prof. Dr. W. Schnick (LMU München) for his continuous support of these investigations.

Appendix A. Supplementary material

Supplementary data associated with this article can be found in the online version at doi:10.1016/j.jssc.2009.12.003.

References

[1] H. Huppertz, B. von der Eltz, J. Am. Chem. Soc. 124 (2002) 9376.
[2] H. Huppertz, Z. Naturforsch. B 58 (2003) 278.
[3] H. Huppertz, H. Emme, J. Phys. Condens. Matter. 16 (2004) 1283.
[4] H. Emme, H. Huppertz, Z. Anorg. Allg. Chem. 628 (2002) 2165.
[5] H. Emme, H. Huppertz, Chem. Eur. J. 9 (2003) 3623.
[6] H. Emme, H. Huppertz, Acta Crystallogr. C 61 (2005) i29.
[7] H. Emme, H. Huppertz, Acta Crystallogr. C 61 (2005) i23.
[8] H. Huppertz, S. Altmannshofer, G. Heymann, J. Solid State Chem. 170 (2003) 320.
[9] H. Emme, M. Valldor, R. Pöttgen, H. Huppertz, Chem. Mater. 17 (2005) 2707.
[10] A. Haberer, G. Heymann, H. Huppertz, J. Solid State Chem. 180 (2007) 1595.
[11] T. Nikelski, Th. Schleid, Z. Anorg. Allg. Chem. 629 (2003) 1017.
[12] T. Nikelski, M.C. Schäfer, H. Huppertz, Th. Schleid, Z. Kristallogr. 233 (2008) 177.
[13] H. Emme, T. Nikelski, Th. Schleid, R. Pöttgen, M.H. Möller, H. Huppertz, Z. Naturforsch. B 59 (2004) 202.
[14] H. Emme, C. Despotopoulou, H. Huppertz, Z. Anorg. Allg. Chem. 630 (2004) 2450.
[15] G. Heymann, T. Soltner, H. Huppertz, Solid State Sci. 8 (2006) 821.
[16] A. Haberer, G. Heymann, H. Huppertz, Z. Naturforsch. B 62 (2007) 759.
[17] G. Corbel, R. Retoux, M. Leblanc, J. Solid State Chem. 139 (1998) 52.
[18] H. Müller-Bunz, Th. Schleid, Z. Anorg. Allg. Chem. 628 (2002) 2750.
[19] A. Haberer, H. Huppertz, J. Solid State Chem. 182 (2009) 888.
[20] A. Haberer, H. Huppertz, Angew. Chem., submitted.
[21] J.S. Knyrim, F. Roeßner, S. Jakob, D. Johrendt, I. Kinski, R. Glaum, H. Huppertz, Angew. Chem. 119 (2007) 9256;
J.S. Knyrim, F. Roeßner, S. Jakob, D. Johrendt, I. Kinski, R. Glaum, H. Huppertz, Angew. Chem. Int. Ed. 46 (2007) 9097.
[22] S.C. Neumair, R. Glaum, H. Huppertz, Z. Naturforsch. B64 (2009) 883.
[23] F.C. Hawthorne, P.C. Burns, J.D. Grice, Reviews in Mineralogy, in: Boron: Mineralogy, Petrology, and Geochemistry, vol. 33, Mineralogical Society of America, Washington, 1996 (Chapter 2).
[24] P.C. Burns, J.D. Grice, F.C. Hawthorne, Can. Miner. 33 (1995) 1131.
[25] D. Walker, M.A. Carpenter, C.M. Hitch, Am. Miner. 75 (1990) 1020.
[26] D. Walker, Am. Miner. 76 (1991) 1092.
[27] H. Huppertz, Z. Kristallogr. 219 (2004) 330.
[28] D.C. Rubie, Phase Transitions 68 (1999) 431.
[29] N. Kawai, S. Endo, Rev. Sci. Instrum. 8 (1970) 1178.
[30] Z. Otwinowski, W. Minor, Methods Enzymol. 276 (1997) 307.
[31] G.M. Sheldrick, SHELXS-97 and SHELXL-97, Program suite for the solution and refinement of crystal structures, University of Göttingen, Göttingen, Germany, 1997.
[32] G.M. Sheldrick, Acta Crystallogr. A 64 (2008) 112.
[33] H. Huppertz, J. Solid State Chem. 177 (2004) 3700.
[34] G. Engel, J. Pretzsch, V. Gramlich, W.H. Baur, Acta Crystallogr. B 31 (1975) 1854.
[35] R. Hoppe, Angew. Chem. 78 (1966) 52;
R. Hoppe, Angew. Chem. Int. Ed. 5 (1966) 96.
[36] R. Hoppe, Angew. Chem. 82 (1970) 7;
R. Hoppe, Angew. Chem. Int. Ed. 9 (1970) 25.
[37] R. Hübenthal, MAPLE-Program for the Calculation of MAPLE Values, Vers. 4, University of Gießen, Gießen, Germany, 1993.
[38] O.J. Guentert, R.L. Mozzi, Acta Crystallogr. 11 (1958) 746.
[39] L.S. Garashina, B.P. Sobolev, V.B. Aleksandrov, Y.S. Vishnyakov, Sov. Phys. Crystallogr. 25 (1980) 171.
[40] C.T. Prewitt, R.D. Shannon, Acta. Crystallogr. B 24 (1968) 869.
[41] P. Becker, Z. Kristallogr. 216 (2001) 523.
[42] K.I. Schaffers, D.A. Keszler, Inorg. Chem. 33 (1994) 1201.
[43] R.W. Smith, D.A. Keszler, J. Solid State Chem. 93 (1991) 430.
[44] R. Norrestam, S. Carlson, A. Sjödin, Acta Crystallogr. C 50 (1994) 1847.
[45] A. Vegas, Acta Crystallogr. B 33 (1977) 3607.
[46] H. Huppertz, Z. Naturforsch. B 56 (2001) 697.
[47] R. Diehl, Solid State Commun. 17 (1975) 743.
[48] E. Zobetz, Z. Kristallogr. 160 (1982) 81.

[49] R. Hoppe, Angew. Chem. 78 (1966) 52;
R. Hoppe, Angew. Chem. Int. Ed. 5 (1966) 96.
[50] R. Hoppe, Angew. Chem. 82 (1970) 7;
R. Hoppe, Angew. Chem. Int. Ed. 9 (1970) 25.
[51] R. Hübenthal, MAPLE—Program for the Calculation of MAPLE Values, Vers. 4, University of Gießen, Gießen, Germany, 1993.
[52] H. Effenberger, F. Pertlik, Z. Kristallogr. 166 (1984) 129.
[53] R.E. Thoma, G.D. Brunton, Inorg. Chem. 5 (1966) 1937.
[54] A. S. Wills, VaList Version 3.0.13, University College London, UK, 1998–2008. Program available from 〈http://www.ccp14.ac.ukwww.ccp14.ac.uk〉.
[55] I.D. Brown, D. Altermatt, Acta Crystallogr. B 41 (1985) 244.
[56] N.E. Brese, M. O'Keeffe, Acta Crystallogr. B 47 (1991) 192.
[57] R. Hoppe, S. Voigt, H. Glaum, J. Kissel, H.P. Müller, K.J. Bernet, Less-Common Met. 156 (1989) 105.
[58] L. Jun, X. Shuping, G. Shiyang, Spectrochim. Acta A 51 (1995) 519.
[59] G. Chadeyron, M. El-Ghozzi, R. Mahiou, A. Arbus, J.C. Cousseins, J. Solid State Chem. 128 (1997) 261.
[60] J.C. Zhang, Y.H. Wang, X. Guo, J. Lumin. 122–123 (2007) 980.
[61] G. Padmaja, P. Kistaiah, J. Phys. Chem. A 113 (2009) 2397.
[62] S. C. Neumair, J. S. Knyrim, O. Oeckler, R. Glaum, R. Kaindl, R. Stalder, H. Huppertz, Chem. Eur. J., submitted.